

# Photophysical Properties of Polypyridyl Carbonyl Complexes of Rhenium(I)

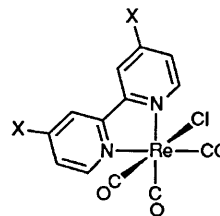
Laura A. Worl, Rich Duesing, Pingyun Chen, Leopoldo Della Ciana and Thomas J. Meyer\*  
 Department of Chemistry, University of North Carolina, Chapel Hill, NC 27599, USA

The photophysical properties of the metal to ligand charge transfer (m.l.c.t.) excited states of the complexes  $[\text{Re}(4,4'\text{-X}_2\text{-bipy})(\text{CO})_3\text{Cl}]$  ( $\text{X} = \text{NH}_2, \text{NEt}_2, \text{NHCOCH}_3, \text{OCH}_3, \text{CH}_3, \text{H}, \text{Ph}, \text{Cl}, \text{CO}_2\text{Et}$  or  $\text{NO}_2$ ; bipy = bipyridine) vary systematically as the substituent X is varied. For the cases where m.l.c.t. states are lowest lying a quantitative correlation exists between  $\ln(k_{\text{nr}} \times 1 \text{ s})$  ( $k_{\text{nr}}$  is the rate constant for non-radiative decay) and the Franck–Condon factor calculated from parameters obtained by emission spectral fitting. The solvent reorganizational energy for  $[\text{Re}(\text{bipy})(\text{CO})_3\text{Cl}]$  has been determined to be  $1100 \text{ cm}^{-1}$  in EtOH–MeOH (4:1 v/v) and  $650 \text{ cm}^{-1}$  in 2-methyltetrahydrofuran by a temperature dependent bandwidth study. Based on a comparative analysis of properties with related polypyridyl complexes of  $\text{Ru}^{\text{II}}$  and  $\text{Os}^{\text{II}}$  it has been concluded that: (1) the extent of distortion at the 4,4'- $\text{X}_2$ -bipy acceptor ligand correlates with the energy gap between the excited and ground states; these results are in agreement with an earlier correlation found for polypyridyl complexes of  $\text{Os}^{\text{II}}$ ; (2) the unusually large Stokes shift and the broadening of the vibronic components in absorption and emission spectra arise from a combination of increased solvent reorganizational energies and greater distortions in the low-frequency modes between the excited and ground states; and (3) the relatively short lifetimes for the complexes of  $\text{Re}^{\text{I}}$  have as a major contributing factor the participation of a  $\nu(\text{CO})$  mode at *ca.*  $2020\text{--}2040 \text{ cm}^{-1}$  as an energy acceptor in non-radiative decay.

For the metal to ligand charge transfer (m.l.c.t.) excited states of polypyridyl complexes of the  $d^6$  metal ions  $\text{Ru}^{\text{II}}$  and  $\text{Os}^{\text{II}}$  the results of photophysical and spectroscopic studies have led to a relatively clear insight into excited state structure and reactivity.<sup>1</sup> At the molecular level the factors that govern non-radiative and radiative decay rate constants, the configurations of the lower lying excited states, the structural differences between the ground and excited states, and the vibrational modes that participate in excited state decay are all becoming more apparent.<sup>2–7</sup>

Polypyridyl complexes of  $\text{Re}^{\text{I}}$  are playing an increasingly important role in studies involving photochemical electron and energy transfers.<sup>8–12</sup> Since the initial investigations by Wrighton and Morse,<sup>8a</sup> the results of a number of studies have appeared based on complexes of the type  $[\text{Re}(\text{bipy})(\text{CO})_3\text{L}]^{n+}$  (bipy = 2,2'-bipyridine). These complexes have been of value in studying medium effects,<sup>13,14</sup> in exploring the fundamental photophysics of m.l.c.t. excited states,<sup>15</sup> and as components of more complex excited state systems including chromophore–quencher complexes.<sup>11,16,17</sup>

An important advantage for the complexes of  $\text{Re}^{\text{I}}$  lies in the availability of a useful synthetic chemistry.<sup>8–10,15,18</sup> Typically, these complexes possess m.l.c.t. excited states which emit and can be monitored by standard emission and lifetime techniques. In this paper we report on the preparation and properties of the series *fac*- $[\text{Re}(4,4'\text{-X}_2\text{-bipy})(\text{CO})_3\text{Cl}]$  ( $\text{X} = \text{NH}_2, \text{NEt}_2, \text{NHCOCH}_3, \text{OCH}_3, \text{CH}_3, \text{H}, \text{Ph}, \text{Cl}, \text{CO}_2\text{Et}$  or  $\text{NO}_2$ ) where the properties of the acceptor ligand are varied systematically by changing the substituent X. The variations in excited state properties that these changes engender have given insight into the role of the acceptor ligand and of substituent changes at that ligand in determining spectroscopic and photophysical properties. In addition, it has been possible to utilize structural and energy parameters for the excited states derived by emission spectral fitting to calculate relative rate constants for non-radiative decay. A comparative analysis of spectroscopic and excited state decay data has revealed the origin of the relatively large Stokes shifts that exist for these complexes and has



identified a  $\nu(\text{CO})$  mode as a major contributor to the relatively short, non-radiative decay lifetimes.

## Experimental

**Materials.**—All reagents were ACS grade and were used without further purification. For emission measurements either 2-methyltetrahydrofuran (mthf) or EtOH–MeOH (4:1 v/v) was used as the solvent. The solvent mthf (Aldrich) was initially passed through an activated column of alumina and then freshly distilled over lithium aluminium hydride; EtOH was freshly distilled over activated Mg turnings. Elemental analyses were performed by Galbraith Laboratories, Knoxville, TN.

**Preparations.**— $[\text{Re}(4,4'\text{-X}_2\text{-bipy})(\text{CO})_3\text{Cl}]$  ( $\text{X} = \text{NEt}_2, \text{NH}_2, \text{NHCOCH}_3, \text{OCH}_3, \text{CH}_3, \text{H}, \text{Cl}, \text{Ph}, \text{CO}_2\text{Et}$  or  $\text{NO}_2$ ). The complexes were prepared from  $[\text{Re}(\text{CO})_5\text{Cl}]$  by the general procedure described below.<sup>18,19</sup> In a typical experiment  $[\text{Re}(\text{CO})_5\text{Cl}]$  (0.50 mmol) and the substituted 2,2'-bipyridine compound (0.50 mmol) in toluene ( $20 \text{ cm}^3$ ) were heated at reflux for 1 h. In most cases a precipitate of the pure compound was formed. This was collected, washed with diethyl ether and dried *in vacuo*. If the substituted 2,2'-bipyridine has lipophilic character (*i.e.*, phenyl) the complex stayed in solution. These complexes were precipitated by slow addition of hexanes. Yields were 80–100%.

Analyses: Found: C, 41.60; H, 4.40; N, 9.25. Calc. for X =

NEt<sub>2</sub>, C<sub>21</sub>H<sub>26</sub>ClN<sub>4</sub>O<sub>3</sub>Re: C, 41.75; H, 4.35; N, 9.25%. Found: C, 32.30; H, 2.20; N, 11.15. Calc. for X = NH<sub>2</sub>, C<sub>13</sub>H<sub>10</sub>-ClN<sub>4</sub>O<sub>3</sub>Re: C, 31.75; H, 2.05; N, 11.40%. Found: C, 41.60; H, 4.40; N, 9.35. Calc. for X = NHC(O)CH<sub>3</sub>: C<sub>17</sub>H<sub>14</sub>ClN<sub>4</sub>O<sub>5</sub>Re: C, 41.75; H, 4.35; N, 9.39%. Found: C, 34.35; H, 2.35; N, 5.45. Calc. for X = OCH<sub>3</sub>, C<sub>15</sub>H<sub>12</sub>ClN<sub>2</sub>O<sub>5</sub>Re: C, 34.50; H, 2.30; N, 5.35%. Found: C, 36.65; H, 2.70; N, 5.70. Calc. for X = CH<sub>3</sub>, C<sub>15</sub>H<sub>12</sub>ClN<sub>2</sub>O<sub>3</sub>Re: C, 36.75; H, 2.45; N, 5.7%. Found: C, 49.25; H, 3.00; N, 4.55. Calc. for X = Ph, C<sub>25</sub>H<sub>16</sub>ClN<sub>2</sub>O<sub>3</sub>Re: C, 48.90; H, 2.65; N, 4.55%. Found: C, 29.30; H, 1.10; N, 5.45. Calc. for X = Cl, C<sub>13</sub>H<sub>6</sub>Cl<sub>3</sub>N<sub>2</sub>O<sub>3</sub>Re: C, 29.40; H, 1.15; N, 5.30%. Found: C, 37.45; H, 2.55; N, 5.60. Calc. for X = CO<sub>2</sub>Et, C<sub>19</sub>H<sub>16</sub>-ClN<sub>4</sub>O<sub>7</sub>Re: C, 37.65; H, 2.65; N, 4.60%.

The preparations of the substituted ligands 4,4'-X<sub>2</sub>-bipy for X = NEt<sub>2</sub>, NH<sub>2</sub>, OCH<sub>3</sub>, Cl or NO<sub>2</sub> have been described previously.<sup>20</sup> For X = NH<sub>2</sub> the quality of the iron powder is very important; Alfa iron powder, 200 mesh was used. The other ligands (X = CH<sub>3</sub>, H or Ph) were commercially available.

4,4'-Bis(ethoxycarbonyl)-2,2'-bipyridine, 4,4'-(CO<sub>2</sub>Et)<sub>2</sub>-bipy. This ligand was prepared in two steps from 4,4'-(CH<sub>3</sub>)<sub>2</sub>-bipy which was first oxidized to 4,4'-(CO<sub>2</sub>H)<sub>2</sub>-bipy by a literature procedure.<sup>21a</sup> The compound 4,4'-(CO<sub>2</sub>H)<sub>2</sub>-bipy (4 g) and SOCl<sub>2</sub> (40 cm<sup>3</sup>) were heated at reflux for 3 h. The excess of SOCl<sub>2</sub> was removed by rotary evaporation and dried overnight under vacuum. A volume of EtOH (4 cm<sup>3</sup>) (distilled over Mg/I<sub>2</sub>) in toluene (50 cm<sup>3</sup>) was added and the mixture was heated at reflux for 2 h. After cooling, CHCl<sub>3</sub> (250 cm<sup>3</sup>) was added. The mixture was extracted twice with 100 cm<sup>3</sup> of H<sub>2</sub>O containing NaHCO<sub>3</sub> (2 g) in order to remove the unreacted 4,4'-(CO<sub>2</sub>H)<sub>2</sub>-bipy. The organic layer was dried with Na<sub>2</sub>SO<sub>4</sub> and the liquids were removed by rotary evaporation. The white solid was recrystallized from Me<sub>2</sub>CO-CHCl<sub>3</sub> (4:1, 50 cm<sup>3</sup> × 2) to give 2.4 g of white crystalline product the nature of which was confirmed by <sup>1</sup>H NMR spectroscopy.<sup>21b</sup>

**Ground State Measurements.**—Cyclic voltammetric measurements were carried out by using a PAR model 173 potentiostat/galvanostat or a PAR 264A polarographic analyser/stripping voltmeter. The measurements utilized a platinum bead working electrode, a platinum wire auxiliary electrode and a saturated sodium chloride calomel reference electrode (SSCE) in a single compartment cell. Spectroscopic grade acetonitrile was used as solvent and tetrabutylammonium hexafluorophosphate (GFS Chemicals) as the supporting electrolyte (0.1 mol dm<sup>-3</sup>). Solutions with dissolved samples (ca. 10<sup>-3</sup> mol dm<sup>-3</sup>) were deaerated by bubbling with N<sub>2</sub> for 10–15 min. A sweep rate of 200 mV s<sup>-1</sup> was used for all scans. The E<sub>1/2</sub> values reported here were obtained as an average of the anodic and cathodic peak potentials, (E<sub>p,a</sub> + E<sub>p,c</sub>)/2. When the oxidative peak potentials were not reversible, an estimated E<sub>1/2</sub> was still obtainable since cathodic return waves of decreased peak currents were still observable.

UV-VIS spectra were recorded by using a Hewlett-Packard model 8451A UV-VIS diode array spectrophotometer. Samples were contained in 1.00 cm quartz cuvettes and were referenced against a solvent blank.

Infrared spectra were recorded on a Nicolet 20DX FTIR instrument in CH<sub>3</sub>CN solution with background subtraction. Raman spectra of solutions of [Re{4,4'-(CH<sub>3</sub>)<sub>2</sub>-bipy}(CO)<sub>3</sub>Cl] were obtained with visible excitation at room temperature. The spectra were collected by a SPEX 1401 double monochromator with excitation from a Spectra Physics 171 Kr<sup>+</sup> laser at Los Alamos National Laboratories by Dr. E. M. Kober.

**Excited State Measurements.**—Samples for lifetime and emission experiments were prepared as optically dilute solutions (ca. 10<sup>-5</sup> mol dm<sup>-3</sup>) in freshly distilled mthf or EtOH-MeOH (4:1 v/v) solutions, freeze-pump-thawed degassed a minimum of four cycles, then sealed under vacuum.

Emission lifetimes were obtained by using a PRA LN1000 pulsed nitrogen laser as the excitation source at 337 nm, and

coupled with a PRA grating LN102/1000 tunable dye head with Exciton dyes Exalite 384 or Bis-MSB for excitation at 384 and 420 nm. The excitation beam was passed through a collection of lenses and defocused onto the sample cell. Either nitromethane or dichromate solution filters were placed before the monochromator to remove scattered laser light. Emission decay was monitored at right angles by using a PRA B204-3 2.5 m monochromator, a Hamamatsu R928 water cooled photomultiplier tube, and a LeCroy 9400 digital oscilloscope, or a Tektronix 7912, or a LeCroy 6880 transient digitizer interfaced to an IBM PC. Reported lifetimes are the averaged result of the analysis of 100–150 decay traces. Lifetimes were obtained by least-squares analysis of the first-order decay of lnI vs. time curves (I = signal intensity) which were linear for at least four half-lives.

Emission spectra were obtained with a SPEX Fluorolog F212 photon counting spectrofluorimeter and corrected for detector sensitivity. For the purposes of spectral fitting and quantum yield measurements, the emission spectra were converted to an abscissa linear in energy as described elsewhere.<sup>22</sup> Emission intensities are reported as the number of quanta emitted per energy interval. Emission quantum yields, φ<sub>em</sub>, were determined at 25.0 ± 0.1 °C by using samples of known absorbance (A < 0.12). The integrated emission profiles were compared to that for a standard sample of [Ru(bipy)<sub>3</sub>][PF<sub>6</sub>]<sub>2</sub> in acetonitrile (φ<sub>em</sub> = 0.062)<sup>23</sup> for complexes with emission manifolds from 600 to 850 nm and to [Re(bipy)(CO)<sub>3</sub>(4-Etpy)]PF<sub>6</sub> in acetonitrile (φ<sub>em</sub> = 0.18)<sup>15</sup> (4-Etpy = 4-ethylpyridine) for complexes with emission manifolds from 550 to 700 nm. Corrections for differences in refractive indices of the solvent and of absorption band intensities were made as described previously.<sup>23</sup> At low temperatures, φ<sub>em</sub> values were calculated by referencing against values at 298 K (φ<sub>298</sub>) by using equation (1),<sup>24,25</sup> where φ<sub>LT</sub> is the emission quantum yield at low

$$\phi_{LT} = \phi_{298} \left( \frac{I_{LT}}{I_{298}} \right) \left( \frac{A_{298}}{A_{LT}} \right) \left( \frac{\eta_{LT}}{\eta_{298}} \right)^2 \quad (1)$$

temperature, I is the integrated intensity of the emission manifold, A is the absorbance at the excitation wavelength and η is the refractive index of the solvent. Where low-temperature absorption measurements were not made, φ<sub>LT</sub> was estimated from equation (2). The simplification follows from the

$$\phi_{LT} = \phi_{298} \left( \frac{I_{LT}}{I_{298}} \right) \quad (2)$$

observation that as the temperature is decreased to 77 K, the fraction A<sub>298</sub>/A<sub>LT</sub> decreases by ca. 16% and (η<sub>LT</sub>/η<sub>298</sub>)<sup>2</sup> increases by ca. 15%.<sup>25</sup> The estimated uncertainties in φ<sub>em</sub> values determined in this manner are ±20%.

Temperature variations for temperature dependent measurements were achieved by using a Janis Research NDT cryostat and Lake Shore Cryogenics DRC 84C temperature controller. Measurements at 77 K were collected with a liquid N<sub>2</sub> quartz finger Dewar [made from Supracil quartz (non-emissive)] and 9 mm diameter glass sample cells adapted for a larger finger Dewar to minimize scattered light.

For emission spectral fitting, a single-mode, Franck-Condon line-shape analysis of the emission spectra was used.<sup>2,25</sup> A VAX 11/780 computer was used for the calculations. The form of the equation used in the fitting procedure is shown in equation (3), where I(ν̄) is the relative emitted light intensity at energy ν̄ in wavenumbers.

$$I(\bar{\nu}) = \sum_{v_M=0}^5 \left[ \left( \frac{E_0 - v_M \hbar \omega_M}{E_0} \right)^3 \times \frac{S_M^{v_M}}{v_M!} \times \exp \left\{ -4 \ln 2 \left[ (\bar{\nu} - E_0 + v_M \hbar \omega_M) / \Delta \bar{\nu}_z \right]^2 \right\} \right] \quad (3)$$

**Table 1** Spectral and electrochemical data for the complexes  $[\text{Re}^{\text{I}}(4,4'\text{-X}_2\text{-bipy})(\text{CO})_3\text{Cl}]$  at  $295 \pm 2$  K

Compound X	$\lambda_{\text{max}}^a/\text{nm}$ ( $10^{-3}\epsilon/\text{dm}^3 \text{ mol}^{-1}$ $\text{cm}^{-1}$ )		$\nu(\text{CO})^b/\text{cm}^{-1}$	$E_{\frac{1}{2}}^c/\text{V}$	
	$\text{CH}_3\text{CN}$	thf		$\text{Re}^{\text{II}}\text{-Re}^{\text{I}}$	bipy-bipy
1 $\text{NEt}_2$	367 (9.79)	375	2014 1903, 1883	1.16 <sup>d</sup>	-1.88
2 $\text{NH}_2$	350 (6.60)	360	2015 1905, 1886	1.16 <sup>d</sup>	-1.83
3 $\text{NHCOCH}_3$	364	385		1.38 <sup>d</sup>	-1.16
4 $\text{OCH}_3$	356 (3.88)	375	2021 1913, 1894	1.28 <sup>d</sup>	-1.46
5 $\text{CH}_3$	364 (3.63)	385	2022 1915, 1897	1.35 <sup>d</sup>	-1.44
6 H	370 (2.45)	400	2023 1917, 1900	1.38 <sup>d</sup>	-1.35
7 Ph	384	410	2022 1918, 1899	1.37	-1.25
8 Cl	390 (3.63)	410	2025 1921, 1904	1.40	-1.11
9 $\text{CO}_2\text{Et}$	412 (4.67)	430	2025 1923, 1906	1.42	-0.96
10 $\text{NO}_2$	448 (4.51)	475	2028 1929, 1912	1.51	-0.45

<sup>a</sup> For the lowest energy absorption maximum. <sup>b</sup> IR absorption maxima in the CO stretching region, in  $\text{CH}_3\text{CN}$  solution. The CO bands appear in two groups: a high intensity band(s) at higher energy, and medium intensity broad bands. <sup>c</sup> Potentials measured in  $0.1 \text{ mol dm}^{-3}$   $[\text{NBu}_4]\text{PF}_6$  in  $\text{CH}_3\text{CN}$  vs. SSCE. Estimated errors are  $\pm 0.04$  V for the couples  $[\text{Re}(4,4'\text{-X}_2\text{-bipy})(\text{CO})_3\text{Cl}]^{+/0}$  and  $\pm 0.01$  V for the couples  $[\text{Re}(4,4'\text{-X}_2\text{-bipy})(\text{CO})_3\text{Cl}]^{0/-}$ . The  $+/0$  couple involves reduction at the polypyridyl ligand. <sup>d</sup> The peak to peak splitting for the oxidation waves were typically 50–180 mV at a scan rate of  $200 \text{ mV s}^{-1}$ . The peak current ratio  $i_{\text{pc}}/i_{\text{pa}}$  was  $< 1$  because of partial chemical re-reduction of  $\text{Re}^{\text{II}}$  by the solvent or of an impurity in the solvent.

**Table 2** Resonantly enhanced Raman frequencies for the ground electronic states of  $[\text{Re}\{4,4'\text{-(CO}_2\text{Et)}_2\text{-bipy}\}(\text{CO})_3\text{Cl}]$  in  $\text{CH}_2\text{Cl}_2$  and thf at  $295 \pm 2$  K following excitation at  $457 \text{ nm}^{a,b}$ 

$\text{CH}_2\text{Cl}_2$	thf
2024vs	2034vs
1634m	1615m
1566s	1546s
1488vs	1498(sh)
1429s	1434(sh)
1332w	1300w
1293m	
1156m	1156m
1039s	
639m	630m
502m	530m
258w	270w

<sup>a</sup> Bands in  $\text{cm}^{-1}$ . <sup>b</sup> Estimated experimental uncertainty is  $\pm 5 \text{ cm}^{-1}$ . Relative intensities are: m = medium, s = strong, w = weak, v = very, sh = shoulder (of solvent band).

One vibrational mode was used in the fits with  $\hbar\omega_{\text{M}}$  ca.  $1450 \text{ cm}^{-1}$ . In equation (3),  $E_0$  is the energy difference between the excited and ground states in their lowest energy vibrational levels. The parameter  $\nu_{\text{M}}$  is the vibrational quantum number for the medium frequency acceptor mode, and  $S_{\text{M}}$  is the corresponding electron-vibrational coupling constant or Huang-Rhys factor.

The emission manifolds of m.l.c.t. excited states of CO-containing complexes of  $\text{Re}^{\text{I}}(\text{bipy})$  are generally non-structured, even at 77 K. From the resonance-Raman data ca. 7  $\nu(\text{bipy})$  vibrational ring stretching modes ( $1000\text{--}1650 \text{ cm}^{-1}$ ) are enhanced. The average value of  $1450 \text{ cm}^{-1}$  used here for  $\hbar\omega_{\text{M}}$  includes contributions from these bands and a  $\nu(\text{CO})$  stretching mode at ca.  $2020\text{--}2040 \text{ cm}^{-1}$ .<sup>7,26,27</sup> In the four parameter fit of the spectral profiles, the parameter  $\Delta\bar{\nu}_{0,\frac{1}{2}}$  includes contributions from low-frequency modes and the solvent.

## Results

**Spectral and Electrochemical Properties.**—In Table 1 are summarized UV-VIS, IR and electrochemical data for the complexes. The complexes share the common feature of having accessible Re-based oxidations and bipyridine-based reductions within the electrochemical limits imposed by the solvent.<sup>19,28</sup> For the amino substituents, the ligand based reduction occurs near the solvent limit. In some cases special features appear in the electrochemistry. For  $[\text{Re}\{4,4'\text{-(CO}_2\text{Et)}_2\text{-bipy}\}(\text{CO})_3\text{Cl}]$  two reduction waves are present. The first wave was chemically

reversible, but cycling through the second led to decomposition and the appearance of new oxidation waves on the return scan. They appear at  $E_{\text{p}} = -0.78$  and  $-1.08$  V. For  $\text{X} = \text{NH}_2$  two quasi-reversible oxidation waves appear. The first oxidation is metal based and occurs at 1.23 V. The second, broader oxidation wave occurs at 1.72 V and is based at the amino groups of the bipy ligand.<sup>29</sup>

As found previously, the absorption maxima are at relatively high energy and overlap somewhat with bipy-based,  $\pi\pi^*$  bands.<sup>8–10,12,30</sup> The lowest energy absorption band (or shoulder) is assigned to a m.l.c.t. transition ( $\text{Re}^{\text{I}} \rightarrow \text{bipy}$ ) with more intense bands (not listed in Table 1) of ligand-based  $\pi\pi^*$  origin occurring at higher energy in the UV region. The m.l.c.t. absorption spectra are sensitive to the nature of the substituents on the polypyridyl ligand. The electron donating substituents increase the energy of the  $\pi^*(4,4'\text{-X}_2\text{-bipy})$  acceptor orbitals to a greater degree than they do the  $d\pi(\text{Re})$  orbitals.

In the IR spectra of the Re complexes, three intense  $\nu(\text{CO})$  modes are observed confirming the facial structures of the complexes.<sup>8,30,31</sup> Table 1. The band at highest energy can be assigned to  $\nu_{\text{sym}}(\text{CO})$  of the carbonyl groups *cis* to the Cl atom.<sup>31</sup> The energies of the CO stretching frequencies also vary with X, with  $\nu(\text{CO})$  shifting to higher energies for electron withdrawing substituents.

In Table 2 are summarized the Raman frequencies that are resonantly enhanced in  $[\text{Re}\{4,4'\text{-(CO}_2\text{Et)}_2\text{-bipy}\}(\text{CO})_3\text{Cl}]$  in tetrahydrofuran (thf) or  $\text{CH}_2\text{Cl}_2$  following excitation into the low-energy portion of the m.l.c.t. manifold at 457 nm. The resonance enhancements that occur in the region  $1000\text{--}1600 \text{ cm}^{-1}$  are attributed to polypyridyl ring stretching modes<sup>26,27</sup> and the band at 2024 or 2034  $\text{cm}^{-1}$  is attributed to the  $\nu(\text{CO})$  stretching mode, as observed previously.<sup>27</sup> The resonantly enhanced CO mode is assigned to a stretching mode of the CO ligand which is *cis* with respect to bipy and *trans* with respect to Cl.<sup>31</sup>

**Emission Spectra and Emission Spectral Fitting.**—In Fig. 1 are shown room-temperature absorbance and emission spectra for the complexes  $[\text{Re}(4,4'\text{-X}_2\text{-bipy})(\text{CO})_3\text{Cl}]$  ( $\text{X} = \text{CO}_2\text{Et}$ ,  $\text{CH}_3$  or  $\text{NH}_2$ ). These spectra illustrate the considerable effect that substituent changes at the chromophoric ligand have on the spectral properties of the complexes. The emission manifolds are broad and structureless even at 77 K except for  $\text{X} = \text{NH}_2$  and  $\text{NEt}_2$ . The 77 K emission spectra of  $[\text{Re}(4,4'\text{-X}_2\text{-bipy})(\text{CO})_3\text{Cl}]$  where  $\text{X} = \text{NEt}_2$ , Cl or Ph and  $[\text{Re}\{4,4'\text{-(NH}_2)_2\text{-bipy}\}(\text{CO})_3(4\text{-Etpy})]^+$  in thf are shown in Fig. 2.

The values of the parameters obtained from the spectral fitting procedure, i.e.  $E_0$ ,  $\hbar\omega_{\text{M}}$ ,  $S_{\text{M}}$  and  $\Delta\bar{\nu}_{0,\frac{1}{2}}$  are collected in

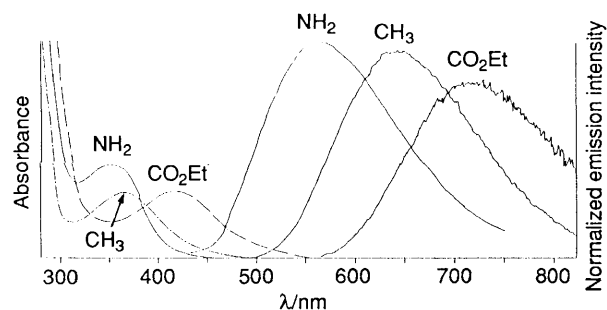


Fig. 1 Electronic absorption and corrected emission spectra in  $\text{CH}_3\text{CN}$  at room temperature for  $[\text{Re}(4,4'\text{-X}_2\text{-bipy})(\text{CO})_3\text{Cl}]$ : X =  $\text{NH}_2$  (—),  $\text{CH}_3$  (---) or  $\text{CO}_2\text{Et}$  (— · — · —), respectively for the absorption spectra, and labelled accordingly for the emission spectra

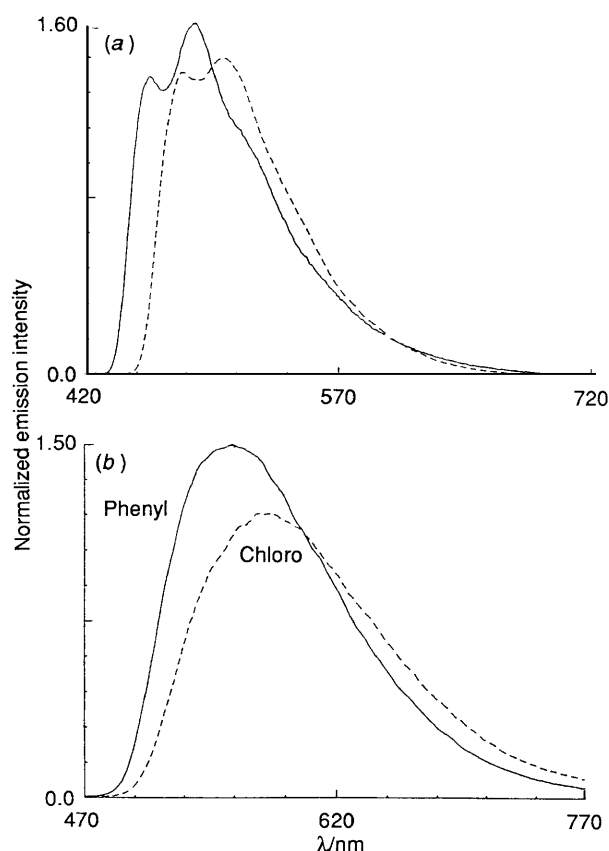


Fig. 2 Corrected emission spectra at 77 K in mthf for (a)  $[\text{Re}\{4,4'\text{-(NH}_2)_2\text{-bipy}\}(\text{CO})_3(4\text{-Etpy})]^+$  (—) and  $[\text{Re}\{4,4'\text{-(NEt}_2)_2\text{-bipy}\}(\text{CO})_3\text{Cl}]$  (---); (b)  $[\text{Re}(4,4'\text{-Ph}_2\text{-bipy})(\text{CO})_3\text{Cl}]$  (—) and  $[\text{Re}(4,4'\text{-Cl}_2\text{-bipy})(\text{CO})_3\text{Cl}]$  (---)

Table 3 for data at room temperature or 160 K. Included in Fig. 3 are the calculated fits for the complexes  $[\text{Re}(4,4'\text{-X}_2\text{-bipy})(\text{CO})_3\text{Cl}]$  where X =  $\text{OCH}_3$  and  $\text{CO}_2\text{Et}$  by using the spectral fitting parameters in Table 3.

Also included in Table 3 are Franck–Condon factors ( $\ln[F(\text{calc.})]$ ) calculated from  $E_0$ ,  $\hbar\omega_M$ ,  $S_M$  and  $\Delta\bar{\nu}_{0,\frac{1}{2}}$ . The quantity  $E_0$  is the band maximum for the first medium frequency progression ( $v_M^* = 0$  to  $v_M = 0$ ) and  $\Delta\bar{\nu}_{0,\frac{1}{2}}$  is the band width at half maximum. It includes contributions from both solvent and low-frequency modes treated semiclassically.<sup>2a</sup> Calculation of Franck–Condon factors was based on a model used previously.<sup>2a</sup> It includes contributions from a medium frequency  $\nu(\text{bipy})$  mode which is an average of seven contributors and the resonantly enhanced  $\nu(\text{CO})$  mode, an averaged low-frequency mode, and the solvent, equation (4).

Table 3 Spectral fitting parameters for  $[\text{Re}(4,4'\text{-X}_2\text{-bipy})(\text{CO})_3\text{Cl}]$  in mthf at 298 and  $160 \pm 2$  K<sup>a</sup>

Compound X	$E_0/\text{cm}^{-1}$	$S_M$	$10^{-3}\Delta\bar{\nu}_{0,\frac{1}{2}}/\text{cm}^{-1}$	$\Delta G_{\text{ES}}^b/\text{cm}^{-1}$	$\ln[F(\text{calc.})]^c$
At 298 K					
1 $\text{NEt}_2$	18 040	1.33	3.2	21 940	−16.1
2 $\text{NH}_2$	18 100	1.33	3.2	22 100	−16.2
3 $\text{NHCOCH}_3$	16 900	1.21	2.7	19 440	−15.9
4 $\text{OCH}_3$	16 340	1.17	3.0	19 600	−15.0
5 $\text{CH}_3$	16 510	1.18	2.9	19 360	−15.4
6 H	16 180	1.15	2.6	18 630	−15.4
7 Ph	15 880	1.05	2.7	18 390	−15.6
8 Cl	14 880	1.00	2.7	17 500	−14.4
9 $\text{CO}_2\text{Et}$	14 300	0.95	2.5	16 370	−14.2
At 160 K					
5 $\text{CH}_3$	16 490	1.20	2.2	19 180	−16.0
6 H	16 380	1.15	2.3	18 790	−16.1
9 $\text{CO}_2\text{Et}$	14 050	0.90	2.2	16 160	−14.6

<sup>a</sup> In the fits,  $\hbar\omega_M = 1450$   $\text{cm}^{-1}$ . Estimated errors were  $E_0$  ( $\pm 5\%$ );  $S_M$  ( $\pm 10\%$ );  $\Delta\bar{\nu}_{0,\frac{1}{2}}$  ( $\pm 15\%$ ). These three parameters are strongly correlated in how they influence the calculated bandshape, equation (3). Our experience has shown that a unique set of parameters cannot be reliably defined if the emission spectra are broad. Appropriate combinations of the parameters in the ranges cited above gave reasonable fits, see references 25, 32b and 33 for details. <sup>b</sup>  $\Delta G_{\text{ES}}$  ( $\pm 3\%$ ) was calculated as  $E_0 + (\Delta\bar{\nu}_{0,\frac{1}{2}})^2/(16k_B T \ln 2)$ . <sup>c</sup>  $\ln[F(\text{calc.})]$  ( $\pm 3\%$ ) was calculated by using equation (4a). The quantities  $\Delta G_{\text{ES}}$  and  $\ln[F(\text{calc.})]$  have relatively small uncertainties compared to those of the individual parameters because the spectral fitting parameters are highly correlated. Those set of spectral fitting parameters that gave a satisfactory representation of the spectrum gave values of  $\Delta G_{\text{ES}}$  and  $\ln[F(\text{calc.})]$  that fell in the ranges cited.

$$\ln[F(\text{calc.})] = -\ln[\hbar\omega_M E_0/(1000 \text{ cm}^{-1})^2]/2 - S_M - \frac{\gamma E_0}{\hbar\omega_M} + (\gamma + 1)^2(\Delta\bar{\nu}_{0,\frac{1}{2}}/\hbar\omega_M)^2/16 \ln 2 \quad (4a)$$

$$\gamma = \ln\left(\frac{E_0}{S_M \hbar\omega_M}\right) - 1 \quad (4b)$$

The Franck–Condon factors are related to the rate constant for non-radiative decay by equation (5),<sup>2a</sup> where  $\beta_0$  is the

$$\ln(k_{\text{nr}} \times 1 \text{ s}) = \ln(\beta_0 \times 1 \text{ s}) + \ln[F(\text{calc.})] \quad (5)$$

vibrationally induced, electronic coupling term and ( $k_{\text{nr}} \times 1 \text{ s}$ ) is dimensionless.

**Excited State Decay.**—Excited state lifetimes were measured at 77 K and at room temperature in mthf. The data are presented in Table 4. As observed for related complexes, a significant shift occurs in the lifetimes at the transition between a frozen glass matrix and a fluid solution.<sup>8a,13,24,32,34,35</sup> There is an additional, slight temperature dependence past the glass to fluid transition and a more marked dependence near room temperature. Lifetimes as a function of temperature were measured for  $[\text{Re}(\text{bipy})(\text{CO})_3\text{Cl}]$  and  $[\text{Re}(\text{bipy})(\text{CO})_3(4\text{-Etpy})]^+$ . For the temperature dependence near room temperature, the data could be fitted to equation (6) where  $k_B$  is the

$$\frac{1}{\tau} = \frac{k_0 + k_1 \exp(-\Delta E_1/k_B T)}{1 + \exp(-\Delta E_1/k_B T)} \quad (6)$$

Boltzmann constant, which is appropriate for two non-degenerate states with a contribution to decay coming from an upper, non-emitting state.<sup>36</sup> In the underlying kinetic model which leads to equation (6), the term  $k_0$  is the Boltzmann averaged value of the decay rate constant from the low-lying,

**Table 4** Excited state properties of  $[\text{Re}^{\text{I}}(4,4'\text{-X}_2\text{-bipy})(\text{CO})_3\text{Cl}]$  in mthf\*

Compound X	$\lambda_{\text{max,em}}/\text{nm}$		$\phi_{\text{em}}$ (295 K)	$\tau/\mu\text{s}$ (77 K)	$\tau/\text{ns}$ (295 K)	$10^4 k_r/\text{s}^{-1}$ (295 K)	$10^6 k_{\text{nr}}/\text{s}^{-1}$ (295 K)
	77 K	295 K					
1 $\text{NEt}_2$	501	575	0.033	12.5	412	7.9	2.4
2 $\text{NH}_2$	502	573	0.020	11.0	262	7.8	3.7
3 $\text{NHCOCH}_3$	535	620	0.0073	4.60	65	11	15
4 $\text{OCH}_3$	525	630	0.0028	3.66	26	10	37
5 $\text{CH}_3$	530	626	0.0057	3.45	49	12	20
6 H	540	642	0.0031	3.12	39	8.0	26
7 Ph	560	647	0.0084	4.36	56	15	18
8 Cl	580	700	0.0006	1.15	9	6.7	110
9 $\text{CO}_2\text{Et}$	598	715	0.0014	2.93	15	9.3	67
10 $\text{NO}_2$	670	780	<0.0001	0.86	<6	1.7	167

\* Estimated errors are  $\lambda_{\text{em}}$  (77 K)  $\pm$  2 nm,  $\lambda_{\text{em}}$  (295 K)  $\pm$  5 nm,  $\phi_{\text{em}}$   $\pm$  10%,  $\tau$   $\pm$  2%,  $\pm$  3 ns for the final three entries.  $\lambda_{\text{max,em}}$  is the emission maximum and  $\phi_{\text{em}}$  the quantum yield for emission.

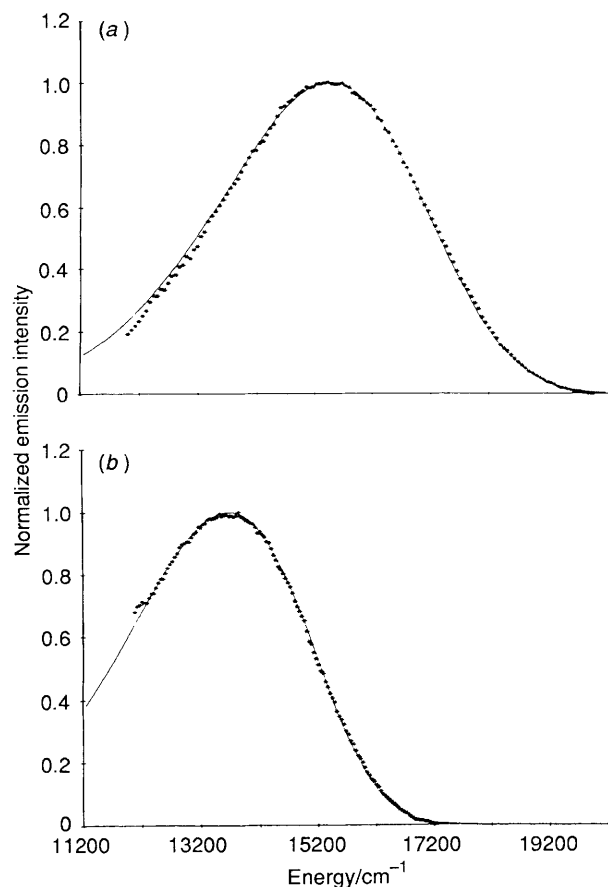


**Fig. 3** Corrected emission spectra (\*) at room temperature in mthf and the calculated fit (—) by using the spectral parameters in Table 3 for the complexes  $[\text{Re}(4,4'\text{-X}_2\text{-bipy})(\text{CO})_3\text{Cl}]$ : (a) X =  $\text{OCH}_3$  and (b) X =  $\text{CO}_2\text{Et}$

initially populated states. It is a composite rate constant which includes both radiative ( $k_1$ ) and non-radiative ( $k_{\text{nr}}$ ) contributions, equation (7). The term  $k_1$  is the rate constant

$$k_0 = k_r + k_{\text{nr}} \quad (7)$$

for decay from the upper state which is assumed to lie at an averaged energy,  $\Delta E_1$ , above the lower states. The term in the denominator of equation (6) is important when  $\Delta E_1 < k_{\text{B}}T$ .<sup>36a</sup> The radiative rate constant is related to  $\phi_{\text{em}}$  as shown in equation (8). The kinetic parameters derived from the fits

$$\phi_{\text{em}} = k_r \tau \quad (8)$$

are collected in Table 5 where they are compared with values obtained for  $[\text{Ru}(\text{bipy})_3]^{2+}$  and  $[\text{Os}(\text{bipy})_3]^{2+}$ .

In earlier studies, the appearance of temperature dependent lifetimes near ambient temperatures was attributed to population and decay *via* higher energy, ligand field (d-d) or m.l.c.t. states.<sup>36a,38</sup> The parameters  $k_1$  and  $\Delta E_1$ , which were obtained from the fits, are of the same order of magnitude for  $[\text{Re}(\text{bipy})(\text{CO})_3\text{Cl}]$  and  $[\text{Os}(\text{bipy})_3]^{2+}$ . Their magnitudes fall in a range consistent with contribution to non-radiative decay by a higher energy m.l.c.t. state or states.<sup>36a</sup> The situation may be the same for  $[\text{Re}(\text{bipy})(\text{CO})_3(4\text{-Etpy})]^+$ , although  $\Delta E_1$  is higher.

## Discussion

A significant feature that emerges from the data presented here is that there is a systematic variation in excited state properties as the substituents X are varied in the 4,4'-X<sub>2</sub>-bipy acceptor ligand. As the properties of the substituents are varied from electron donating ( $\text{NH}_2$ ,  $\text{NET}_2$ ) to electron withdrawing ( $\text{NO}_2$ ,  $\text{CO}_2\text{Et}$ ), both the maximum in the m.l.c.t. absorption band manifold and the emission energy shift to lower energy. It has been observed elsewhere that correlations exist between these shifts and the Hammett parameters  $\sigma_p$ .<sup>15b</sup>

It is possible to understand the electronic origins of the shifts based on simple bonding arguments. The m.l.c.t. transitions involve electronic excitations (or de-excitations) between donor orbitals that are largely  $d\pi$  in character to (or from) acceptor orbitals that are largely  $\pi^*(\text{bipy})$  in character. As shown by the ligand-based reduction potentials in Table 1, the acceptor ability of the  $\pi^*$  orbitals is enhanced with the increasing electron withdrawing character of X. This effect is transmitted to the  $d\pi$  orbitals by backbonding *via*  $d\pi-\pi^*(\text{bipy})$  mixing. As can be inferred from the  $E_{\frac{1}{2}}$  values for the  $\text{Re}^{\text{II}}-\text{Re}^{\text{I}}$  couples in Table 1, there is a corresponding decrease in the ability of  $\text{Re}^{\text{I}}$  to act as a reductant as X becomes more electron withdrawing. This arises from an increase in  $d\pi-\pi^*$  backbonding which makes the metal more electron deficient. As might have been expected, the effect is less profound at the  $d\pi$  orbitals than at the  $\pi^*$  orbitals since the substituent changes are made at the ligand. The range of  $E_{\frac{1}{2}}$  values for the  $\text{Re}^{\text{II}}-\text{Re}^{\text{I}}$  couples is 0.35 V ( $\text{NH}_2$  to  $\text{NO}_2$ ) while the range in  $E_{\frac{1}{2}}$  values for the ligand-based reductions is 1.43 V over the same range of substituents. The backbonding effect is also transmitted to the CO ligand. As  $d\pi-\pi^*(\text{bipy})$  backbonding increases,  $d\pi-\pi^*(\text{CO})$  backbonding decreases as shown by the increase in frequencies for the CO stretching vibrations (Table 1).

Because of the influence of the CO ligands on  $\text{Re}^{\text{I}}$ , there is a relatively large energy separation between the  $d\pi(\text{Re})$  and  $\pi^*(4,4'\text{-X}_2\text{-bipy})$  orbitals compared to typical polypyridyl complexes of  $\text{Ru}^{\text{II}}$  and  $\text{Os}^{\text{II}}$ . The greater separation in energy leads to decreased mixing between the  $d\pi$  and  $\pi^*$  orbitals,

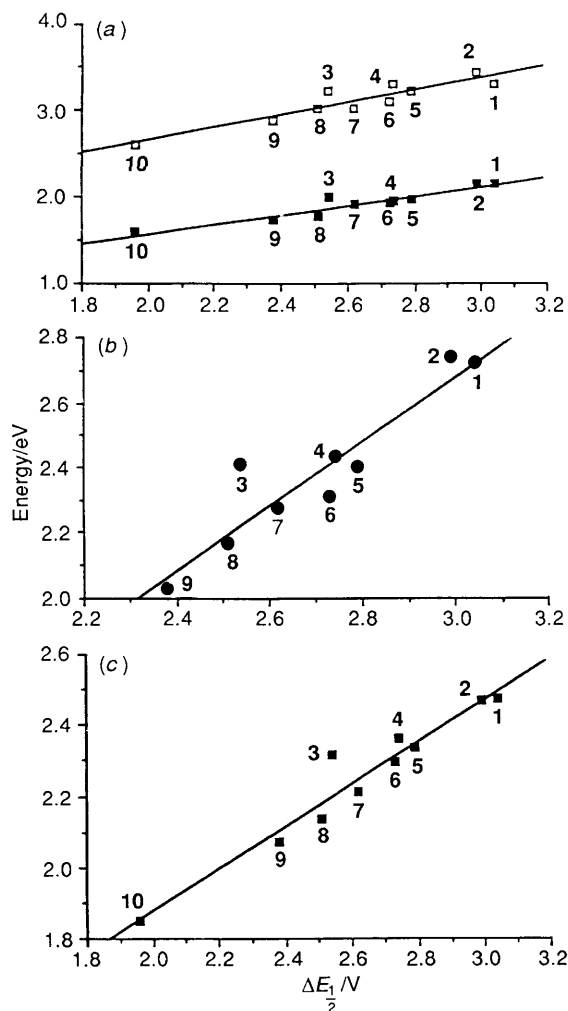


**Fig. 4** (a) Variations of absorption ( $\square$ ) or emission ( $\blacksquare$ ) energies at 295 K and (b) of emission energies at 77 K in a mthf glass ( $\bullet$ ) with  $\Delta E_{\frac{1}{2}}$  (in  $\text{CH}_3\text{CN}-0.1 \text{ mol dm}^{-3} [\text{NBu}_4]\text{PF}_6$ ). The lines are the least-squares fit to linear correlations. The slopes of the correlations are 0.73 for the absorption data and 0.52 for the emission data in (a). (c) Variations in  $\Delta G_{\text{ES}} = E_0 + (\Delta\bar{\nu}_{0,3})^2 / [(16\ln 2)k_{\text{B}}T]$  with  $\Delta E_{\frac{1}{2}}$ . The slope and intercept of the correlation are 0.92 and  $-1.53$  respectively. The data for the complexes in which there were amino substituents were not included in the correlations. The data and numbering scheme are from Tables 1, 3 and 4

decreased oscillator strengths for the m.l.c.t. transitions, decreased radiative decay constants, and high excited to ground state energy gaps. In earlier correlations involving polypyridyl complexes of  $\text{Ru}^{\text{II}}$  or  $\text{Os}^{\text{II}}$ , it has been found that the energy gap is the key parameter to understanding excited state properties, *i.e.* non-radiative lifetimes, redox potentials and excited state structure.<sup>2,39</sup> This conclusion emerged from studies on closely related families of complexes where systematic changes were made in the chromophoric or non-chromophoric ligands. An analysis of the photophysical data presented here reveals that the energy gap plays the same role in the CO-containing complexes of  $\text{Re}^{\text{I}}$ . The results of this analysis also give insight into the origin of two features that distinguish these complexes from complexes of  $\text{Ru}^{\text{II}}$  and  $\text{Os}^{\text{II}}$ . These are Stokes shifts that are relatively large and lifetimes for non-radiative decay that are unusually short.

**Excited State Properties: Absorption and Emission.**—The m.l.c.t. spectra of the Re complexes are broad and featureless because of increased band widths and spectral compression caused by the relatively high energies of the transitions. In lower energy  $\text{Os}^{\text{II}}$  absorbers such as  $[\text{Os}(\text{bipy})_3]^{2+}$ , some structure is

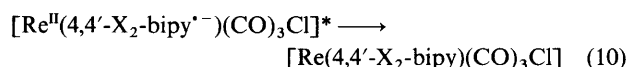
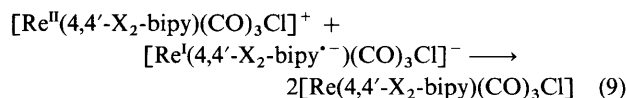
observed in the spectra even at room temperature and transitions to m.l.c.t. states that are largely triplet in character are observed at low energy.<sup>40,41</sup> From the non-Gaussian shapes of the low-energy absorption manifolds for  $[\text{Re}(4,4'\text{-X}_2\text{-bipy})(\text{CO})_3\text{Cl}]$ , Fig. 1, low-energy transitions to m.l.c.t. states that are largely triplet in character may also occur in these spectra. If they do, they are badly convoluted with transitions that are largely singlet in character and have higher intensities. Because of the large spin-orbit coupling constants at Re (*ca.*  $1000 \text{ cm}^{-1}$ ), the 'singlet' and 'triplet' m.l.c.t. excited states are expected to be highly mixed.

It is a characteristic feature of m.l.c.t. absorption and emission band energies that they display linear correlations with ground state redox potentials.<sup>1,19,39,42,43</sup> The basis for these correlations lies in the fact that the same metal-centred and ligand-centred orbitals that are involved in the m.l.c.t. transition are also involved in the oxidation-reduction processes that are measured electrochemically. These relationships also exist for the complexes of  $\text{Re}^{\text{I}}$ . In Fig. 4(a) are shown plots of absorption or emission maxima (Tables 1 and 4) *vs.*  $\Delta E_{\frac{1}{2}} = E_{\frac{1}{2}}(\text{Re}^{\text{II}}-\text{Re}^{\text{I}}) - E_{\frac{1}{2}}(\text{bipy}^0-\text{bipy}^-)$ . The points for the substituents  $\text{X} = \text{NHC}(\text{O})\text{CH}_3$ ,  $\text{NH}_2$  or  $\text{NMe}_2$  were excluded from the correlations. The excited state properties of the complexes that have amino substituents are complex and appear to involve more than one state having different orbital origins.<sup>38b</sup>

The slopes of the plots in Fig. 4(a) and 4(b) are less than unity. This is because the emission and absorption energies include contributions from outer-sphere ( $\lambda_0$ ) and inner-sphere ( $\lambda_i$ ) reorganizational energies ( $E_{\text{abs}} \approx \Delta G + \lambda$ ;  $E_{\text{em}} \approx \Delta G - \lambda$ ) and  $\lambda$  increases with the energy gap between the excited and ground states.<sup>29,30,33,34</sup>

In Fig. 4(c) is shown a plot of  $\Delta G_{\text{ES}} \{ \approx E_0 + (\Delta\bar{\nu}_{0,3})^2 / [(16\ln 2)k_{\text{B}}T] \}$  *vs.*  $\Delta E_{\frac{1}{2}}$ . The quantity  $\Delta G_{\text{ES}}$ , which was calculated from the parameters obtained by emission spectral fitting, is approximately equal to the free energy content of the excited state above the ground state.<sup>2,44,45</sup> The slope of this correlation is much closer to unity even though electrochemical and emission data were acquired in different solvents.

The free energy changes associated with  $\Delta E_{\frac{1}{2}}$  [equation (9)] and  $\Delta G_{\text{ES}}$  [equation (10)] are those for comproportionation of



the oxidized and reduced complexes and decay of the excited state to the ground state, respectively. From the near unity correlation in Fig. 4(c), the effect of the changes in X on electronic structure in the ground state are transferred to the excited states in an intact manner.

Assuming that m.l.c.t. absorption and emission involve orbitally related singlet and triplet states, the apparent average 'Stokes shift,' the energy difference between absorption and emission maximum, is *ca.*  $10\,000 \text{ cm}^{-1}$  from the difference in intercept between the two linear correlations in Fig. 4(a). The same quantity is *ca.*  $6000 \text{ cm}^{-1}$  for  $[\text{Ru}(\text{bipy})_3]^{2+}$  or *ca.*  $6600 \text{ cm}^{-1}$  for  $[\text{Os}(\text{bipy})_3]^{2+}$ .<sup>41</sup> The difference between the absorption and emission maxima depends upon the energy difference between the orbitally equivalent singlet and triplet states,  $\Delta E_{\text{S-T}}$ , and the reorganization energy, equation (11). As

$$E_{\text{abs}} - E_{\text{em}} \sim E_{\text{S-T}} + 2\lambda \quad (11)$$

shown in a later section, up to *ca.*  $2500 \text{ cm}^{-1}$  of the difference in Stokes shift between  $[\text{Re}(\text{bipy})(\text{CO})_3\text{Cl}]$  and  $[\text{Os}(\text{bipy})_3]^{2+}$  arises from a larger contribution to  $\lambda$  from low-frequency vibrational modes and the solvent.

**Changes in Structure at the Acceptor Ligand.**—The results of

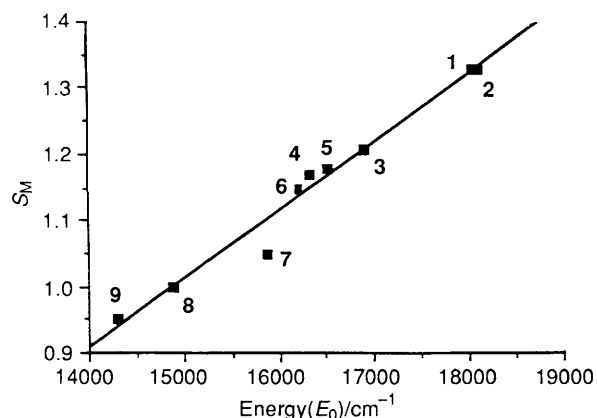


Fig. 5 Variation of  $S_M$  values with  $E_0$ . The linear correlation for the complexes of Re has a slope of  $1.0 \times 10^{-4}$

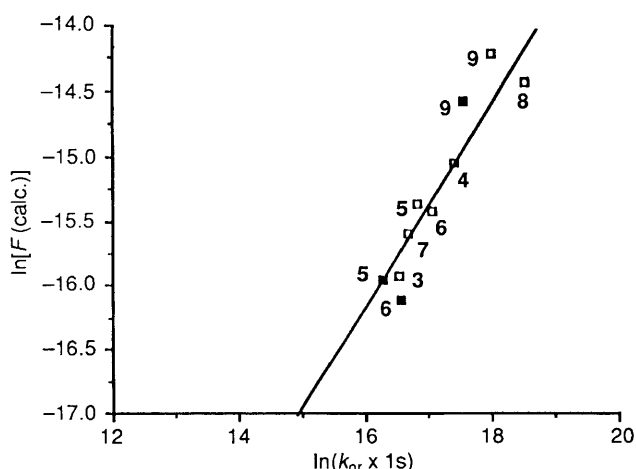


Fig. 6 Plot of the observed value of  $\ln(k_{nr} \times 1 \text{ s})$  vs.  $\ln[F(\text{calc.})]$  at room temperature ( $\square$ ), and selected examples at 160 K ( $\blacksquare$ ). In the linear correlation, a slope of 1 was imposed. The intercept is  $-32.4$ . The data and numbering scheme are given in Tables 3 and 4

emission spectral fitting give insight into the effect that changes in X have on the structure of the bipy acceptor ligand in the excited state. The resonance enhancements for the series of  $\nu(\text{bipy})$  bands that appear in the region  $1000\text{--}1650 \text{ cm}^{-1}$ , Table 2, are found for other polypyridyl complexes of  $\text{Ru}^{\text{II}}$ ,  $\text{Os}^{\text{II}}$  or  $\text{Re}^{\text{I}}$ .<sup>7,26,27,31</sup> For  $[\text{Re}\{4,4'-(\text{CO}_2\text{Et})_2\text{-bipy}\}(\text{CO})_3\text{Cl}]$ , an additional,  $\nu(\text{CO})$  mode appears at  $2024 \text{ cm}^{-1}$  in  $\text{CH}_2\text{Cl}_2$  or  $2034 \text{ cm}^{-1}$  in thf. The contribution made by this mode to the emission spectral profile is incorporated into the emission spectral fitting parameters as an increase in  $\hbar\omega_M$  from  $1350 \text{ cm}^{-1}$ , which is typical for polypyridyl complexes of  $\text{Ru}^{\text{II}}$  and  $\text{Os}^{\text{II}}$ ,<sup>2a</sup> to  $1450 \text{ cm}^{-1}$ .

Satisfactory fits of the emission spectral profiles were made by assuming a common pattern of acceptor vibrations through the series  $4,4'\text{-X}_2\text{-bipy}$ . The same observation was made earlier for the series  $[\text{Ru}(\text{tpm})(4,4'\text{-X}_2\text{-bipy})(\text{py})]^{2+}$  [tpm = tris(pyrazol-1-yl)methane, py = pyridine].<sup>39b</sup> This fact points to a common pattern of bipy-based acceptor modes as X is varied.

A linear correlation exists between  $S_M$  and the energy gap,  $E_0$ , Fig. 5. The quality of the correlation in Fig. 5 is somewhat deceiving given the uncertainties cited in the footnotes to Table 3. The electron-vibrational coupling constant is related to the change in equilibrium displacement between the excited and ground states ( $\Delta Q_e$ ) for the average  $\nu(\text{bipy})$  mode, as shown in equation (12), where  $M$  is the reduced mass and  $\omega$  the angular frequency.

$$S_M = \frac{1}{2}(M\omega_M/\hbar)(\Delta Q_e)^2 \quad (12)$$

From the plot in Fig. 5,  $S_M$  increases by *ca.*  $10^{-4}$  per  $1 \text{ cm}^{-1}$  increase in the energy gap. By assuming a reduced mass of 13 and that the skeletal changes are shared equally over the C–N and C–C bonds in the rings, this corresponds to an increase in average C–N, C–C bond distance of  $0.017\text{--}0.020 \text{ \AA}$  over the series  $\text{X} = \text{CO}_2\text{Et}$  to  $\text{NH}_2$ .<sup>2,39</sup> An increase in the change in average bond length with the energy gap is commonly observed. As the energy gap is increased, the extent of charge transfer increases. This increases the distortion in the acceptor ligand.

The sensitivity of  $S_M$  to  $E_0$  is comparable to sensitivities found in the series  $[\text{Os}(\text{bipy})(\text{L})_4]^{2+}$  ( $\text{L} = \frac{1}{2}\text{bipy}$ , py,  $\text{CH}_3\text{CN}$  or  $\frac{1}{2}\text{Ph}_2\text{PCH}_2\text{CH}_2\text{PPh}_2$  etc.), where  $\delta S_M/\delta E_0 = 1.1 \times 10^{-4} \text{ cm}^{-2a}$ . From the agreement between the two sets of data,<sup>2c</sup> it can be concluded that changes induced in  $S_M$  (and  $\Delta Q_e$ ) by the energy gap are roughly comparable and independent of whether the metal ion is  $\text{Re}^{\text{I}}$  or  $\text{Os}^{\text{II}}$ .

Even with this agreement, there is an anomaly. In the series  $[\text{Ru}(\text{tpm})(4,4'\text{-X}_2\text{-bipy})(\text{py})]^{2+}$ ,  $\delta S_M/\delta E_0 = 1.7 \times 10^{-4} \text{ cm}^{-2}$ . Structural changes in the excited states of these complexes are more sensitive to the energy gap. The difference between the  $\text{Re}^{\text{I}}$  and  $\text{Ru}^{\text{II}}$  series is not understood in a detailed way. It may have its origin in compensating electronic effects in the  $\text{Re}^{\text{I}}$  complexes induced by changes in backbonding to the CO ligands.

*Non-radiative Decay.*—The variations induced by the changes in X extend to excited state lifetimes, Table 4. Since  $\varphi_{em} < 0.03$  for each case (Table 4), the lifetimes are dictated by non-radiative decay and  $1/\tau \approx k_{nr}$ . It is apparent from the data that these lifetimes decrease as the energy gap between the excited and ground states decrease. It is possible to explain this effect quantitatively by using equations (4) and (5) and the results of emission spectral fitting in Table 3.

In non-radiative decay, a transition occurs between states that, to zero order, cannot mix, with the release of a large amount of energy. The transition is induced by a molecular vibration or vibrations which mix the states and is the origin of the term  $\beta_0$  in equation (5). The electronic energy released in the transition appears in the molecular vibrations of the molecule and the librations of the surrounding solvent. Only those modes in which there is a change in equilibrium displacement or frequency between states can participate as energy acceptors. In equation (4), the terms  $S_M + \gamma E_0/\hbar\omega_M$  include the contribution of the medium frequency  $\nu(\text{bipy})$  modes. They dominate as energy acceptors. The term containing  $\Delta\tilde{\nu}_{0,\frac{1}{2}}$  includes contributions from low-frequency modes, treated classically, and the solvent.

If radiative and non-radiative decay occur from, or are dominated by, the same excited state, these parameters can be evaluated from the emission spectra. According to equation (4) if the electronic coupling term  $\beta_0$  remains constant,  $\ln(k_{nr} \times 1 \text{ s})$  should vary linearly with the Franck–Condon factor  $\ln[F(\text{calc.})]$ . These factors can be calculated once the parameters  $S_M$ ,  $E_0$ ,  $\hbar\omega_M$  and  $\Delta\tilde{\nu}_{0,\frac{1}{2}}$  are known by emission spectral fitting, Table 3. In Fig. 6 is shown a plot of  $\ln(k_{nr} \times 1 \text{ s})$  vs.  $\ln[F(\text{calc.})]$ . The plot excludes the data for the amino cases,  $\text{X} = \text{NH}_2$  or  $\text{NEt}_2$ . No attempt was made to correct the lifetime data for contributions to non-radiative decay by upper states. For the cases where the temperature dependence of  $\tau$  was investigated, Table 5, contributions from these states are relatively small at room temperature. However, non-radiative decay from these states may be an important contributor to the scatter in the plot in Fig. 6.<sup>39c</sup>

In constructing the linear correlation in Fig. 6, a slope of 1 was imposed. The intercept of the correlation is  $-32.4$ . The correlations include data taken for three of the complexes at two different temperatures, 160 and 298 K. Based on the linear relationship that is found between  $\ln(k_{nr} \times 1 \text{ s})$  and  $\ln[F(\text{calc.})]$ , it can be inferred that  $\ln\beta_0$  does remain reasonably constant throughout the series. This implies that the electronic orbital

**Table 5** Kinetic parameters for excited state decay

Complex	<i>T</i> /K	Solvent	<i>k</i> <sub>0</sub> <sup>a</sup> /s <sup>-1</sup>	<i>k</i> <sub>0</sub> <sup>a</sup> /s <sup>-1</sup>	$\Delta E_1^a$ /cm <sup>-1</sup>
[Re(bipy)(CO) <sub>3</sub> (4-Etpy)]PF <sub>6</sub>	180–295	4:1 EtOH–MeOH	$(3.40 \pm 0.05) \times 10^6$	$(1.8 \pm 0.3) \times 10^8$	1130 ± 50
[Re(bipy)(CO) <sub>3</sub> Cl]	140–295	mthf	$(5.40 \pm 0.02) \times 10^6$	$(4.9 \pm 0.3) \times 10^7$	270 ± 15
[Re(bipy)(CO) <sub>3</sub> Cl]	160–295	4:1 EtOH–MeOH	$(5.46 \pm 0.06) \times 10^6$	$(5.9 \pm 0.5) \times 10^7$	250 ± 24
[Ru(bipy) <sub>3</sub> ] <sup>2+</sup> <sup>b</sup>	150–330	4:1 EtOH–MeOH	$0.50 \times 10^6$	$2.0 \times 10^{14}$	4040
[Os(bipy) <sub>3</sub> ] <sup>2+</sup> <sup>c</sup>	210–298	4:1 EtOH–MeOH	$3.7 \times 10^6$	$7.2 \times 10^7$	312

<sup>a</sup> From fits of the temperature dependent lifetime data to equation (6). <sup>b</sup> From ref. 37. <sup>c</sup> From ref. 36.

character of the excited state or states that dominate non-radiative decay is the same throughout the series.

It is possible to calculate the vibronically induced, electronic interaction integral,  $V_k$ , from the vibrationally induced electronic coupling term,  $\beta_0$ , by using equation (13),<sup>2a</sup> where

$$\beta_0 = (C_k^2 \omega_k)(1s)(\pi/2)^{1/2}/(1000 \text{ cm}^{-1}) \\ = (V_k^2/\hbar)(1s)(2\pi)^{1/2}/(1000 \text{ cm}^{-1}) \quad (13)$$

$\hbar\omega_k$  is the frequency or averaged frequency of the promoting mode or modes which mix the ground and excited states. By assuming that metal–ligand stretching or bending modes of  $\hbar\omega = ca. 300 \text{ cm}^{-1}$  serve in this role, a value of  $V_k = ca. 600 \text{ cm}^{-1}$  can be calculated. This value is comparable to  $V_k = ca. 1300 \text{ cm}^{-1}$  determined in the same way for the series of Os<sup>II</sup>(bipy) complexes alluded to above.<sup>2a</sup>

In comparing polypyridyl complexes of Os<sup>II</sup> with members of the series [Re(4,4'-X<sub>2</sub>-bipy)(CO)<sub>3</sub>Cl], which have comparable energy gaps, the Re-based excited states are shorter-lived. For example, lifetimes for [Os(bipy)<sub>2</sub>(dppe)]<sup>2+</sup>\* (dppe = Ph<sub>2</sub>-PCH<sub>2</sub>CH<sub>2</sub>PPh<sub>2</sub>;  $E_0 = 15990 \text{ cm}^{-1}$ )<sup>36a</sup> and [Re(bipy)(CO)<sub>3</sub>Cl]\* ( $E_0 = 16180 \text{ cm}^{-1}$ ) in EtOH–MeOH (4:1 v/v) at 160 K, where contributions to non-radiative decay by upper states is negligible, are 880 and 65 ns respectively.

An important contributing factor to the decreased lifetime for the complex of Re<sup>I</sup> comes from the participation of the  $\nu(\text{CO})$  stretching vibration as an energy acceptor. The evidence for the involvement of this mode comes from resonance-Raman data, Table 2, and the increase from 1350 to 1450  $\text{cm}^{-1}$  for  $\hbar\omega_M$  in emission spectral fitting. Based on equations (4) and (5), an increase in  $\hbar\omega_M$  of this magnitude at an energy gap of 16000  $\text{cm}^{-1}$  would result in an increase in  $k_{nr}$  by a factor of ca. 3–4. The origin of the effect lies in the added energy acceptor capability of the  $\nu(\text{CO})$  mode.<sup>15a</sup>

Qualitative energy gap correlations, in which  $\ln(k_{nr} \times 1\text{s})$  has been shown to vary linearly with  $E_0$ , have been found for m.l.c.t. excited states of Os<sup>II</sup> and Ru<sup>II</sup>.<sup>2,23–25,46</sup> For these complexes, varying the energy gap by making variations in non-chromophoric ligands, the solvent, counter ions, or the glass to fluid transition all give slopes of  $\delta \ln(k_{nr} \times 1\text{s})/\delta E_0$  or  $\delta \ln(k_{nr} \times 1\text{s})/\delta E_{em}$  of  $0.8 \times 10^{-3}$  to  $-0.9 \times 10^{-3}$ . For the series of Re complexes, the slopes of plots of  $\ln(k_{nr} \times 1\text{s})$  vs.  $E_0$  are  $\delta \ln(k_{nr} \times 1\text{s})/\delta E_0 = -(0.91 \pm 0.05) \times 10^{-3}$  and  $\delta \ln(k_{nr} \times 1\text{s})/\delta E_{em} = -(0.86 \pm 0.09) \times 10^{-3}$ . In an earlier study based on complexes of the type [Re(bipy)(CO)<sub>3</sub>L]<sup>+</sup> (L = NCCH<sub>3</sub>, PMe<sub>3</sub> or py etc.), where the energy gap was varied by varying the non-chromophoric ligand L, the magnitude of the slope was considerably larger,  $-1.5 \times 10^{-3}$ .<sup>15a</sup>

**Low Frequency Modes and the Solvent.**—The contributions to the emission spectral profile by low-frequency modes and the solvent are included in the band width parameter  $\Delta\bar{\nu}_{0,\frac{1}{2}}$ . Low-

frequency modes broaden the  $\nu(\text{bipy})$  vibronic components by adding additional vibronic transitions. In turn the solvent broadens each of the individual vibronic transitions.

Compared to polypyridyl complexes of Ru<sup>II</sup> or Os<sup>II</sup>, the band widths of the individual vibronic components are unusually broad for the complexes of Re<sup>I</sup>. The bandwidths are so broad that individual  $\nu(\text{bipy})$  vibronic components cannot be observed even at 77 K in frozen solution, Fig. 2(b). Although vibronic structure is observed for the amino cases, X = NH<sub>2</sub> or NEt<sub>2</sub>, Fig. 2(a), as noted above, the excited state structure of these complexes are complicated and the origin of the emission is not clear.<sup>38b</sup> The complexes [Re{4,4'-(CH<sub>3</sub>)<sub>2</sub>-bipy}(CO)<sub>3</sub>Cl] and [Ru(bipy)<sub>3</sub>]<sup>2+</sup> have comparable emission energies, 626 and 635 nm in mthf, respectively.\* From the results of emission spectral fitting in mthf,  $\Delta\bar{\nu}_{0,\frac{1}{2}}$  ca. 2880  $\text{cm}^{-1}$  for [Re{4,4'-(CH<sub>3</sub>)<sub>2</sub>-bipy}(CO)<sub>3</sub>Cl]. For [Ru(bipy)<sub>3</sub>]<sup>2+</sup>,  $\Delta\bar{\nu}_{0,\frac{1}{2}}$  ca. 1400  $\text{cm}^{-1}$ .\*

In principle, it is possible to separate the contributions to  $\Delta\bar{\nu}_{0,\frac{1}{2}}$  from low-frequency modes and the solvent by temperature dependent studies. The band width is related to the solvent reorganizational energy  $\chi_0$ , and the temperature by the relationship in equation (14), where the contribution from the low-frequency modes is treated as an averaged mode of spacing  $\hbar\omega_L$  and electron vibrational coupling constant  $S_L$ . The term  $\Delta\bar{\nu}_{0,\frac{1}{2}}^0$  is the contribution to the half band width from inhomogeneous broadening.<sup>47</sup> Elsewhere, the contributions from the solvent and low-frequency modes have been separated by using the spectral fitting procedure.<sup>2c</sup> The squares of the resulting band widths, equation (14a), are plotted vs.  $T$  in Fig. 7

$$(\Delta\bar{\nu}_{0,\frac{1}{2}})^2 = (\Delta\bar{\nu}_{0,\frac{1}{2}}^0)^2 + 8 \ln 2 \left[ S_L (\hbar\omega_L)^2 \coth \left( \frac{\hbar\omega_L}{2k_B T} \right) + 2k_B T \chi_0 \right] \quad (14)$$

$$(\Delta\bar{\nu}_{\frac{1}{2}})^2 = (\Delta\bar{\nu}_{0,\frac{1}{2}}^0)^2 + 16 \ln k_B T \chi_0 \quad (14a)$$

$$(\Delta\bar{\nu}_{\frac{1}{2}})^2 \sim C + (7.71\chi_0)T \quad (15)$$

for [Re(bipy)(CO)<sub>3</sub>Cl] in EtOH–MeOH (4:1 v/v) or mthf. There are large uncertainties in the individual values of  $\Delta\bar{\nu}_{\frac{1}{2}}$ , see footnote to Table 3. The quality of the correlation in Fig. 7 arises because the temperature dependence of the low-frequency mode was included in the fits and the remaining spectral fitting parameters are relatively insensitive to changes in  $T$ . The rate of change of  $\Delta\bar{\nu}_{\frac{1}{2}}$  with  $T$  is reasonably well defined.

From the slopes of the plots,  $\chi_0 = 1100 \pm 120 \text{ cm}^{-1}$  in EtOH–MeOH (4:1 v/v) and  $650 \pm 40 \text{ cm}^{-1}$  in mthf. The value in EtOH–MeOH is considerably higher than values found for [Os(bipy)(dppen)<sub>2</sub>]<sup>2+</sup> (dppen = *cis*-Ph<sub>2</sub>PCH=CHPPh<sub>2</sub>;  $\chi_0 = 470 \text{ cm}^{-1}$ ) or [Os(bipy)<sub>2</sub>(dppe)]<sup>2+</sup> ( $\chi_0 = 390 \text{ cm}^{-1}$ ) in the same solvent.<sup>33,36a</sup>

By comparing the values for  $\Delta\bar{\nu}_{0,\frac{1}{2}}$  and  $\chi_0$  in mthf, it is apparent that the contribution to the band width from the low-frequency modes is considerable. From these data and equation (14),  $S_L \hbar\omega_L = ca. 2000 \text{ cm}^{-1}$ . For the complexes of Os<sup>II</sup>,  $S_L \hbar\omega_L = 1000 \text{ cm}^{-1}$  for [Os(bipy)(dppen)<sub>2</sub>]<sup>2+</sup> and 800  $\text{cm}^{-1}$  for [Os(bipy)<sub>2</sub>(dppe)]<sup>2+</sup>.

In these complexes the absence of vibronic structure and the relatively large Stokes shifts come from two sources. One is the

\* The emission spectral fitting parameters for [Ru(bipy)<sub>3</sub>]<sup>2+</sup> in mthf at 298 K:  $E_0 = 16100 \text{ cm}^{-1}$ ,  $\hbar\omega_M = 1375 \text{ cm}^{-1}$ ,  $S_M = 1.0$ ,  $\hbar\omega_L = 400 \text{ cm}^{-1}$ ,  $S_L = 1.4$  and  $\Delta\bar{\nu}_{\frac{1}{2}} = 1350 \text{ cm}^{-1}$ . These parameters are the results of a six parameter fit which includes an average low frequency mode ( $S_L \hbar\omega_L$ ) and the solvent ( $\Delta\bar{\nu}_{\frac{1}{2}}$ ).<sup>2</sup>

**Table 6** Excited state properties in mthf<sup>a</sup>

Compound	$\lambda_{\max,em}/\text{nm}$		$\phi_{em}^b$ (160 K)	$\tau/\mu\text{s}$ (77 K)	$\tau/\text{ns}$ (160 K)	$10^4 k_r/\text{s}^{-1}$ (160 K)	$10^6 k_{nr}^c/\text{s}^{-1}$ (160 K)
	77 K	160 K					
[Re{4,4'-(NEt <sub>2</sub> ) <sub>2</sub> -bipy}(CO) <sub>3</sub> (4-Etpy)]PF <sub>6</sub>	470	494		13.00			
[Re{4,4'-(NEt <sub>2</sub> ) <sub>2</sub> -bipy}(CO) <sub>3</sub> Cl]	512	555	0.1250	12.52	1369	9.1	6.39
[Re{4,4'-(NH <sub>2</sub> ) <sub>2</sub> -bipy}(CO) <sub>3</sub> Cl]	510	538	0.1540	11.05	9004	1.7	0.94
[Re{4,4'-(CH <sub>3</sub> ) <sub>2</sub> -bipy}(CO) <sub>3</sub> Cl]	530	630	0.0102	3.450	85	12.0	11.64
[Re(bipy)(CO) <sub>3</sub> Cl]	535	642	0.0045	3.123	65	6.9	15.32
[Re{4,4'-(CO <sub>2</sub> Et) <sub>2</sub> -bipy}(CO) <sub>3</sub> Cl]	600	715	0.0019	2.933	24	7.9	41.59

<sup>a</sup> Estimated errors are  $\lambda_{em}$  (77 K)  $\pm 2\%$ ,  $\lambda_{em}$  (160 K)  $\pm 10\%$ ,  $\phi_{em}$   $\pm 15\%$ ,  $\tau \pm 5$  ns. <sup>b</sup> Calculated from  $\phi_{298}(I_{LT}/I_{298})(A_{298}/A_{LT})(\eta_{LT}/\eta_{298})^2$ , see text. <sup>c</sup> Determined from  $\phi_{em}$  (160 K) and lifetime from equations (6)–(8).

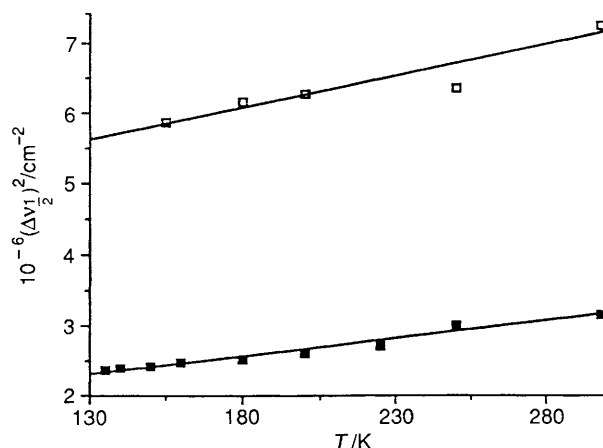


**Fig. 7** Plots of  $(\Delta\bar{\nu}_{1/2})^2$  vs.  $T$  for [Re(bipy)(CO)<sub>3</sub>Cl] in 4:1 EtOH–MeOH (□) and mthf (■). The linear correlations have slopes of 8480 (□) and 4960 (■)  $\text{cm}^{-2} \text{K}^{-1}$  and intercepts of  $4.5 \times 10^6$  (□) and  $1.7 \times 10^6$   $\text{cm}^{-2}$  (■). Data were taken from ref. 2c

greater solvent reorganizational energy that exists between the excited and ground states. The second is an increased contribution from low-frequency modes. The origin of this effect may lie in greater distortions in the metal–ligand skeletal framework perhaps through greater changes in equilibrium displacement for the M–CO modes.

The increased contributions to  $\Delta\bar{\nu}_{0,1/2}$  from low-frequency modes and the solvent also appear as an enhanced contribution to non-radiative decay. The magnitude of the effect can be calculated by using equations (4) and (5). By using an energy gap of 16 000  $\text{cm}^{-1}$  and an increase in  $\Delta\bar{\nu}_{0,1/2}$  from 1400 to 2800  $\text{cm}^{-1}$ , there is an enhancement in  $k_{nr}$  from this effect of ca. 1.5. As the extent of reorganization of solvent in the excited state increases, it plays a more important role as an energy acceptor as do the low-frequency modes as  $\Delta Q_e$  increases.

## Conclusion

A number of conclusions have been reached concerning the photophysical properties of the emitting m.l.c.t. states of [Re(4,4'-X<sub>2</sub>-bipy)(CO)<sub>3</sub>Cl] and how their properties compare to related polypyridyl complexes of Ru<sup>II</sup> and Os<sup>II</sup>.

1. In this co-ordination environment the separation between the  $d\pi(\text{Re})$  and  $\pi^*(4,4'\text{-X}_2\text{-bipy})$  orbitals is high. This leads to enhanced excited-ground state energy gaps, decreased  $d\pi\text{-}\pi^*$  mixing, decreased oscillator strengths, and decreased  $k_r$  values.
2. Absorption and emission spectra are broad and featureless because of relatively large contributions to the spectral profiles from low-frequency molecular modes and solvent librations.
3. The large energy differences that exist between absorbance and emission maxima (Stokes shift) arise from enhanced reorganizational energies for the low-frequency modes and the

4. Linear correlations exist between absorption and emission energies and the difference in redox potentials for the corresponding  $\text{Re}^{\text{II}}\text{-Re}^{\text{I}}$  and  $(4,4'\text{-X}_2\text{-bipy})^0\text{-}(4,4'\text{-X}_2\text{-bipy})^-$  couples.
5. The extent of distortion in the 4,4'-X<sub>2</sub>-bipy ligand in the excited state increases linearly with the energy gap between the excited and ground states. These data fall roughly on the same correlation as one found earlier for complexes of Os<sup>II</sup>.
6. From results obtained by resonance-Raman and emission spectral fitting, a contribution to the emission spectral profile exists from a  $\nu(\text{CO})$  mode at 2024  $\text{cm}^{-1}$  in  $\text{CH}_2\text{Cl}_2$ . This mode, along with the usual  $\nu(\text{bipy})$  ring stretching modes, plays a major role as energy acceptor in non-radiative decay.
7. From the results of a temperature dependent band width study, the solvent reorganizational energy for [Re(bipy)(CO)<sub>3</sub>Cl]\* is 1100  $\text{cm}^{-1}$  in EtOH–MeOH (4:1 v/v) compared to 470  $\text{cm}^{-1}$  for [Os(bipy)(dppen)<sub>2</sub>]<sup>2+</sup> or 390  $\text{cm}^{-1}$  for [Os(bipy)<sub>2</sub>(dppe)]<sup>2+</sup>. The reorganizational energy for the average low-frequency, skeletal vibrations is ca. 2000  $\text{cm}^{-1}$ .
8. A quantitative energy gap correlation exists between rate constants for non-radiative decay and Franck–Condon factors calculated by using parameters obtained by emission spectral fitting.
9. The major factor leading to decreased lifetimes of ca. 10 for the Re-based m.l.c.t. excited states compared to polypyridyl complexes of Os<sup>II</sup> having the same energy gap is in the participation of a relatively high frequency,  $\nu(\text{CO})$  mode as an energy acceptor in non-radiative decay. An additional factor is an enhanced contribution from low-frequency modes and the solvent.

## Acknowledgements

Acknowledgement is made to the Department of Energy under Grant No. DE-FG05-86ER13633 for support of this research. The authors also thank Drs. E. M. Kober for collecting the Raman spectra and K. Barqawi for several initial lifetime measurements and Ms. D. K. Graff for calculating some spectral fitting parameters.

## References

- 1 A. Juris, V. Balzani, F. Barigelletti, F. Campagna, P. Belser and A. Von Zelewsky, *Coord. Chem. Rev.*, 1988, **84**, 85; K. Kalyanasundaram, *Coord. Chem. Rev.*, 1982, **46**, 159; T. J. Meyer, *Pure Appl. Chem.*, 1986, **58**, 1193; E. Krausz and J. Ferguson, *Prog. Inorg. Chem.*, 1989, **37**, 293; R. J. Watts, *J. Chem. Educ.*, 1983, **60**, 834; G. A. Crosby, K. A. Highland and K. A. Truesdell, *Coord. Chem. Rev.*, 1985, **64**, 41; M. K. DeArmond, K. W. Hanck and D. W. Wertz, *Coord. Chem. Rev.*, 1985, **65**, 65.
- 2 (a) E. M. Kober, J. V. Caspar, R. S. Lumpkin and T. J. Meyer, *J. Phys. Chem.*, 1986, **90**, 3722; (b) J. V. Caspar, T. D. Westmoreland, G. H. Allen, P. G. Bradley, T. J. Meyer and W. H. Woodruff, *J. Am. Chem. Soc.*, 1984, **106**, 3492; (c) L. A. Worl, Ph.D. Thesis, University of North Carolina, Chapel Hill, 1989; (d) E. M. Kober and T. J. Meyer, *Inorg. Chem.*, 1984, **23**, 3877; (e) E. M. Kober and T. J. Meyer, *Inorg. Chem.*, 1985, **24**, 106.
- 3 Y. Komada, S. Yamauchi and N. Hirota, *J. Phys. Chem.*, 1988, **92**, 6511.
- 4 C. Creutz, M. Chou, T. L. Netzel, M. Okumura and M. Sutin, *J. Am. Chem. Soc.*, 1980, **102**, 1309.

- 5 S. J. Milder, J. S. Gold and D. S. Kliger, *J. Phys. Chem.*, 1986, **90**, 548.
- 6 T. Hiraga, N. Kitamura, H. B. Kim, S. Tazuke and N. Mōri, *J. Phys. Chem.*, 1989, **93**, 2940.
- 7 P. G. Bradley, N. Kress, B. A. Hornberger, R. F. Dallinger and W. H. Woodruff, *J. Am. Chem. Soc.*, 1981, **103**, 7441.
- 8 (a) M. S. Wrighton and D. L. Morse, *J. Am. Chem. Soc.*, 1974, **96**, 998; (b) G. L. Geoffroy and M. S. Wrighton, *Organometallic Photochemistry*, Academic Press, New York, 1979.
- 9 A. Juris, S. Campagna, I. Bidd, J.-M. Lehn and R. Ziessel, *Inorg. Chem.*, 1988, **27**, 4007; W. Kaim, H. E. A. Kramer, C. Vogler and J. Reiker, *J. Organomet. Chem.*, 1989, **367**, 107.
- 10 K. Kalyanasundaram, *J. Chem. Soc., Faraday Trans. 2*, 1986, 2401.
- 11 T. D. Westmoreland, K. S. Schanze, P. E. Neveux, jun, E. Danielson, B. P. Sullivan, P. Chen and T. J. Meyer, *Inorg. Chem.*, 1985, **24**, 2596; P. Chen, E. Danielson and T. J. Meyer, *J. Phys. Chem.*, 1988, **92**, 3708; P. Chen, T. D. Westmoreland, E. Danielson, K. S. Schanze, D. Anthon, P. Neveux, jun. and T. J. Meyer, *Inorg. Chem.*, 1987, **26**, 1116.
- 12 B. P. Sullivan, *J. Phys. Chem.*, 1989, **93**, 24.
- 13 H. G. Drickamer and O. A. Salman, *J. Chem. Phys.*, 1982, **77**, 3337.
- 14 G. A. Reitz, W. J. Dressick, J. N. Demas and B. A. Degraff, *J. Am. Chem. Soc.*, 1986, **108**, 5344; G. A. Reitz, J. N. Demas and B. A. Degraff, *J. Am. Chem. Soc.*, 1988, **110**, 5051.
- 15 (a) J. V. Caspar and T. J. Meyer, *J. Phys. Chem.*, 1983, **87**, 952; (b) J. K. Hino, L. Della Ciana, W. J. Dressick and B. P. Sullivan, unpublished work.
- 16 G. Tapolsky, R. Duesing and T. J. Meyer, *J. Phys. Chem.*, 1989, **93**, 3885.
- 17 P. Chyongjin, I. Koichiro and S. Yanagida, *Chem. Lett.*, 1989, **5**, 765; T. A. Perkins, D. B. Pourreau, T. L. Netzel and K. S. Schanze, *J. Phys. Chem.*, 1989, **93**, 4511.
- 18 J. C. Luong, Ph.D. Dissertation, Massachusetts Institute of Technology, 1981.
- 19 J. V. Caspar, B. P. Sullivan and T. J. Meyer, *Inorg. Chem.*, 1984, **23**, 2104; B. P. Sullivan and T. J. Meyer, *J. Chem. Soc., Chem. Commun.*, 1984, 403.
- 20 G. Maerker and F. H. Case, *J. Am. Chem. Soc.*, 1953, **80**, 2745; R. B. Woodward and D. Wenkert, *J. Org. Chem.*, 1983, **48**, 283.
- 21 (a) K. D. Bos, J. G. Kraijkamp and J. G. Noltes, *Synth. Commun.*, 1979, **9**, 497; (b) P. Chen, unpublished work.
- 22 C. A. Parker and W. T. Rees, *Analyst (London)*, 1960, **85**, 857; G. H. Allen, R. P. White, D. P. Rillema and T. J. Meyer, *J. Am. Chem. Soc.*, 1984, **106**, 2613.
- 23 J. V. Caspar and T. J. Meyer, *J. Am. Chem. Soc.*, 1983, **105**, 5583; J. V. Caspar, Ph.D. Dissertation, University of North Carolina, Chapel Hill, 1987.
- 24 R. S. Lumpkin and T. J. Meyer, *J. Phys. Chem.*, 1986, **90**, 5307.
- 25 R. S. Lumpkin, Ph.D. Dissertation, University of North Carolina, Chapel Hill, 1987.
- 26 O. Poizat and C. Sourisseau, *J. Phys. Chem.*, 1984, **88**, 3007.
- 27 P. A. Mabrouk and M. S. Wrighton, *Inorg. Chem.*, 1986, **25**, 526; W. K. Smothers and M. S. Wrighton, *J. Am. Chem. Soc.*, 1983, **105**, 1067.
- 28 B. P. Sullivan, C. M. Bolinger, D. Conrad, W. J. Vining and T. J. Meyer, *J. Chem. Soc., Chem. Commun.*, 1985, 1414.
- 29 L. D. Margerum, Ph.D. Dissertation, University of North Carolina, Chapel Hill, 1985.
- 30 P. J. Giordano and M. S. Wrighton, *J. Am. Chem. Soc.*, 1979, **101**, 2888.
- 31 R. W. Balk, D. J. Stufkens and A. Oskam, *J. Chem. Soc., Dalton Trans.*, 1981, 1124.
- 32 (a) L. A. Worl and T. J. Meyer, *Chem. Phys. Lett.*, 1988, **143**, 541; (b) L. A. Worl, Ph.D. Dissertation, University of North Carolina, Chapel Hill, 1989.
- 33 L. A. Worl, R. S. Lumpkin, J. V. Caspar, Z. Murtaza, E. M. Kober and T. J. Meyer, unpublished work.
- 34 J. Van Houten and R. J. Watts, *J. Am. Chem. Soc.*, 1976, **98**, 4853; T. J. Kemp, *Prog. React. Kinetics*, 1980, **10**, 301.
- 35 F. Barigelletti, P. Belser, A. Von Zelewsky, A. Juris and V. Balzani, *J. Phys. Chem.*, 1985, **89**, 3680; F. Barigelletti, A. Juris, V. Balzani, P. Belser and A. Von Zelewsky, *J. Phys. Chem.*, 1986, **90**, 5190.
- 36 (a) R. S. Lumpkin, E. M. Kober, L. A. Worl, Z. Murtaza and T. J. Meyer, *J. Phys. Chem.*, 1990, **94**, 239; (b) T. Azumi, C. M. O'Donnell and S. P. McGlynn, *J. Chem. Phys.*, 1966, **45**, 2735.
- 37 F. Barigetti, V. Balzani, P. Belser and A. Von Zelewsky, *Inorg. Chem.*, 1983, **22**, 3335.
- 38 (a) B. Durham, J. V. Caspar, J. K. Nagle and T. J. Meyer, *J. Am. Chem. Soc.*, 1982, **104**, 4803; (b) R. Duesing, L. A. Worl, P. Chen and T. J. Meyer, unpublished work.
- 39 (a) E. M. Kober, J. L. Marshall, W. J. Dressick, B. P. Sullivan, J. V. Caspar and T. J. Meyer, *Inorg. Chem.*, 1985, **24**, 2755; (b) K. R. Barqawi, A. Llobet and T. J. Meyer, *J. Am. Chem. Soc.*, 1988, **110**, 7751; (c) Z. Murtaza, K. R. Barqawi and T. J. Meyer, *J. Phys. Chem.*, 1991, **95**, 47.
- 40 V. Balzani, F. Bolletta, M. T. Gandolfi and M. Maestri, *Top. Curr. Chem.*, 1978, **75**, 1.
- 41 E. M. Kober and T. J. Meyer, *Inorg. Chem.*, 1982, **21**, 3967; E. M. Kober and T. J. Meyer, *Inorg. Chem.*, 1980, **102**, 4102; E. M. Kober, J. V. Caspar, B. P. Sullivan and T. J. Meyer, *Inorg. Chem.*, 1988, **27**, 4587.
- 42 F. Barigelletti, A. Juris, V. Balzani, P. Belser and A. Von Zelewsky, *Inorg. Chem.*, 1987, **26**, 4115; A. Juris, S. Campagna, V. Balzani, G. Gremaud and A. Von Zelewsky, *Inorg. Chem.*, 1988, **27**, 3652.
- 43 P. Ghosh and A. Chakravorty, *Inorg. Chem.*, 1984, **23**, 2242; E. S. Dodsworth and A. B. P. Lever, *Chem. Phys. Lett.*, 1986, **124**, 152.
- 44 B. S. Brunschwigg, S. Ehrenson and N. Sutin, *J. Phys. Chem.*, 1987, **91**, 4714.
- 45 R. A. Marcus, *J. Phys. Chem.*, 1989, **93**, 3078.
- 46 W. J. Vining, J. V. Caspar and T. J. Meyer, *J. Phys. Chem.*, 1985, **89**, 1095; J. V. Caspar, E. M. Kober, B. P. Sullivan and T. J. Meyer, *J. Am. Chem. Soc.*, 1982, **104**, 630; J. V. Caspar and T. J. Meyer, *Inorg. Chem.*, 1983, **22**, 2444.
- 47 C. J. Ballhausen, *Molecular Electronic Structures of Transition Metal Complexes*, McGraw-Hill, New York, 1979, ch. 4.

Received 3rd October 1990; Paper 0/04462H